Ann. Rev. Fluid Mech. 1983. 15:123–47

AUTOROTATION[1]

Hans J. Lugt

David W. Taylor Naval Ship Research and Development Center, Bethesda, Maryland 20084

1. INTRODUCTION

The subject of autorotation has been a stepchild in fluid dynamics. It is barely mentioned in textbooks and considered more a curiosity than a topic for serious study. Some people have even labeled autorotation as "toy aerodynamics," a notion that is certainly not justified. Once, autorotation was expected to be of importance in the understanding of flying, particularly in studying airfoils, but this idea died quickly. Later, autorotation gained interest in various unrelated areas such as flight dynamics of aircraft, aeroballistics, biology, meteorology, and sports. The diversity of these application areas is part of the reason for the lack of a uniform treatment, for the difficulty in collecting literature, and for the variances in the definition of autorotation. Another reason for the lack of a comprehensive treatment is the difficulty, both experimental and theoretical, of obtaining qualitative data and in explaining autorotation satisfactorily. Imagine trying to measure the surface pressure on a rotating piece of cardboard falling in air! The theoretical difficulties are indicated by the fact that autorotation is essentially a nonlinear phenomenon associated with vortex shedding. Analogies exist to vortex-induced vibrations of bodies, a subject area that has attracted more attention in the past than autorotation. All of these problems are addressed in this review.

[1]The US Government has the right to retain a nonexclusive royalty-free license in and to any copyright covering this paper.

2. DEFINITION

The concept of autorotation is not uniquely defined in fluid dynamics. Sometimes, aerodynamicists consider any continuous rotation of a body in a parallel flow without external sources of energy as autorotation. Under this definition, windmills, waterwheels, anemometers, and certain tree fruits and seeds are "autorotating" devices. These bodies are geometrically shaped in such a way that, whenever they are kept fixed in a fluid flow, a torque is created that initiates rotation as soon as the bodies are released. Examples of this kind of "pseudo-autorotation" are given in Figure 1.

On the other hand, a body can exhibit autorotation proper [in the classical sense of Riabouchinsky (1935), who introduced the term "autorotation" in 1906] only if one or more stable positions exist at which the fluid flow exerts no torque on the resting body. In this case, a sufficiently strong initial impulse is required before the fluid flow can sustain a continuous spinning of the body.

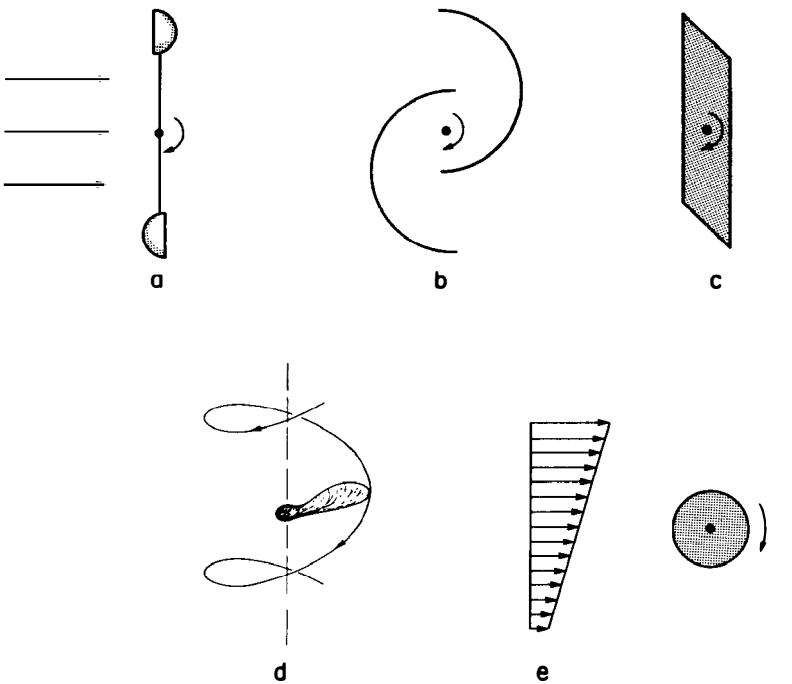

Figure 1 Pseudo-autorotation. (*a*) Cup-anemometer; (*b*) Savonius rotor (cross section); (*c*) Riabouchinsky plate (cross section); (*d*) maple seed; (*e*) cylinder rotating due to shear flow.

Although the axis of rotation may assume any orientation with respect to the flow, it is useful theoretically and didactically to distinguish two special cases of axis orientation for autorotation in the restricted, classical sense. In the first special case, the axis of rotation is parallel to the flow, and the body must be symmetrical with regard to the parallel stream so that no torque is present when the body is at rest. This state is generally stable. An initial impulse is then necessary to obtain autorotation. Typical examples are the Lanchester propeller and the spinning airfoil (Figure 2).

In the second special case, the axis is perpendicular to the parallel flow and the body need be symmetrical with respect to the parallel flow in only one stable position (Lugt 1980). In this position the flow exerts no torque on the resting body, and again an initial impulse is necessary to obtain autorotation. However, other positions may exist from which the body will start rotating when released with no initial impulse, provided the body can pick up and store sufficient angular momentum to overcome the adverse torque around the stable position. The fundamental difference between the two cases of autorotation may also be expressed in this way: While the rate of stable autorotation is essentially constant for bodies autorotating parallel to the flow (provided the wake of the body is fairly constant), the rate of autorotation in the other case is basically periodic.

Examples of bodies autorotating perpendicular to the flow are the falling rectangular piece of cardboard and the rotating dumbbell (Figure 3). Actually, the axis of the cardboard (or plate) may be free to move or may be fixed in a parallel stream. Other symmetrically shaped bodies that can autorotate are also shown in Figure 3. A word of caution is in order here with respect to symmetry properties. Whereas bodies displaying pseudo-autorotation have only axial symmetry (if any at all), the bodies in Figure 3 have both axial and plane symmetry. For example, the Savonius rotor in Figure 1 has a twofold axial symmetry but the triangle in Figure 3 has threefold axial and plane symmetry.

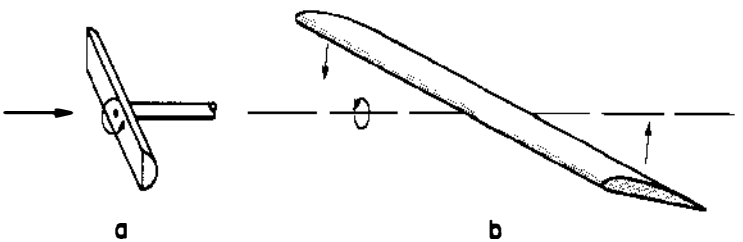

Figure 2 Bodies autorotating parallel to the flow. (*a*) Lanchester propeller; (*b*) autorotating airfoil.

For irregularly shaped bodies, the difference between pseudo-autorotation and autorotation proper is not always clear and can depend on the position of the axis of rotation and the flow situation. For instance, the cup anemometer in Figure 1 has a point between the geometric center and the cup facing the stream at which the body is in a stable equilibrium for a certain Reynolds-number range. Also, the autorotation of airplanes and reentry bodies can border on pseudo-autorotation. The situation is even further obscured when the axis of rotation can assume any orientation with respect to the flow (Figure 4). Hence it is sometimes unavoidable to trespass into the gray area between pseudo-autorotation and classical autorotation. In this review, the word autorotation is used in the classical sense.

The application areas of autorotation are manifold. The principles of the Lanchester propeller and the autorotating wing are basic for the

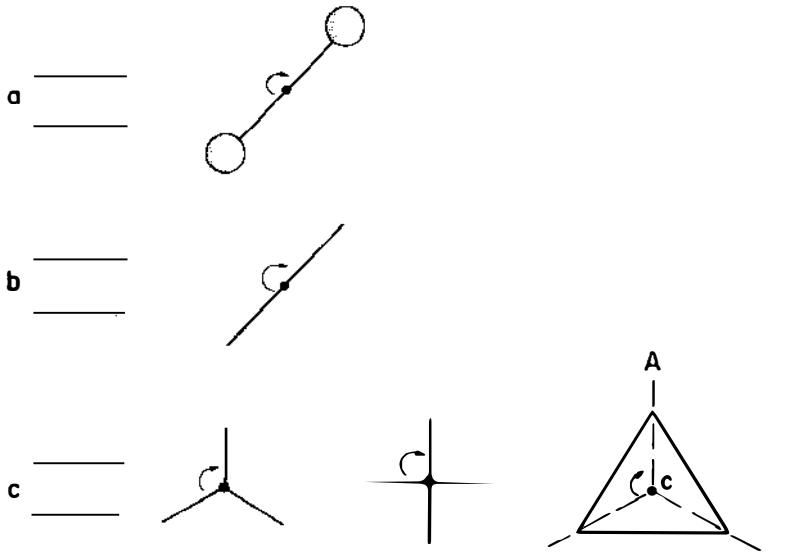

Figure 3 Bodies autorotating perpendicular to the flow. (*a*) Rotating dumbbell; (*b*) rotating plate; (*c*) examples of Magnus rotors. *A-C* line of lateral symmetry

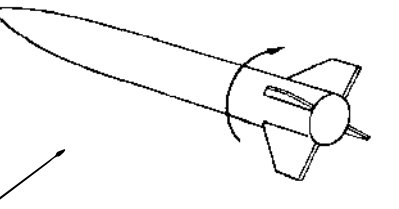

Figure 4 Autorotating finned missile.

understanding of spinning aircraft (Jones 1963). The free-falling autorotating plate is exemplified in nature by certain tree fruits and seeds (McCutchen 1977) and its fall characteristics are used in aeroballistics to predict dispersion patterns for the distribution of leaflets and bomblets (Burgess 1967) or to study fragmentation of the flying body. Autorotating missiles with cruciform fins pose a control problem, and the same is true for autorotating reentry bodies and disposable nose sections of aircraft (Cohen et al. 1974, A. M. O. Smith 1953). Autorotating plates have also been proposed for deceleration and high-lift devices (Neumark 1963, Iversen 1969, Miller 1973). In meteorology the growth of hailstones of oblate spheroidal shape is affected by autorotation (Kry & List 1974b).

3. AUTOROTATION PARALLEL TO THE FLOW

Autorotation of bodies about an axis parallel to the flow is in general easier to explain and more amenable to a quantitative description than autorotation perpendicular to the flow. The reason is that the fluid motion is steady in the stable state for a body-fixed reference frame. In almost all theoretical considerations, the two-dimensional strip method is used. Then, the local angle of attack changes due to the rotational velocity $V = R\Omega$ according to

$$\Delta\alpha = \tan^{-1} p, \qquad p = \frac{V}{U} \tag{1}$$

where U is the constant speed of the parallel flow, R the radius or half-span of the wing-type body, Ω the angular velocity, and p the roll parameter. The total angle of attack α of a flow against a blade element is then $\alpha_0 + \Delta\alpha$, with α_0 the angle of attack for $V = 0$.

The aerodynamic forces support rotation if $V/U = p > L/D$, where L and D are the lift and drag, respectively (Figure 5). To meet this criterion, the total angle of attack must be in the region of stall so that the slope $dL/d\alpha$ becomes negative and its absolute value according to Glauert (1919) so large that the condition

$$\frac{dL}{d\alpha} + D < 0 \tag{2}$$

is satisfied. The local condition (2) for a blade element need not be met everywhere along the span as long as the integration over the whole span results in a torque in the direction of rotation.

The Lanchester propeller and the rotating wing are now explained in detail on the basis of this steady-state strip theory.

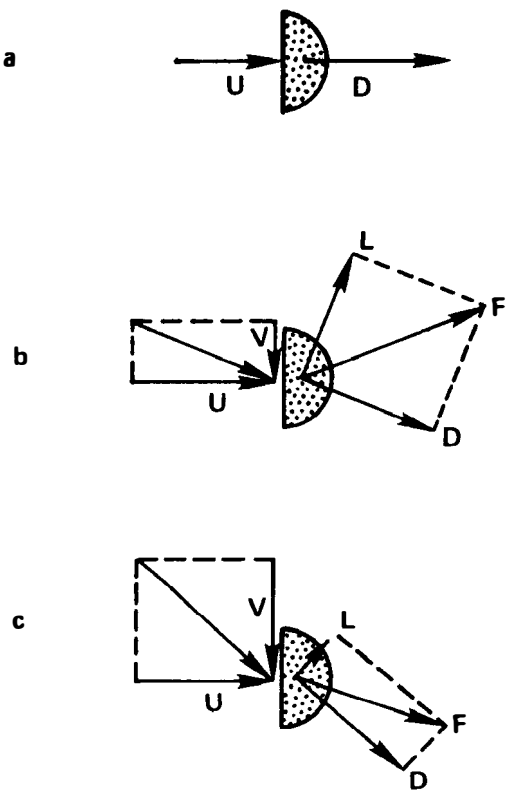

Figure 5 Forces on a D-shaped blade element of the Lanchester propeller.

3.1 Lanchester Propeller

The forces acting on the Lanchester propeller (Figure 2*a*) are depicted in Figure 5 for a D-shaped blade element. Without rotation, only a drag force D is present (*a*). A slowly rotating blade causes a lift L; the resultant F opposes rotation (*b*). Thus, any slow initial rotation ceases in time. If, however, the initial rotation is large enough, the resultant force can support rotation (*c*). The propeller starts autorotating and increases its angular velocity until a steady equilibrium with the damping force is reached.

Applying the steady-state strip theory to the Lanchester propeller, one must set $\alpha_0 = 90°$. The slope $dL/d\alpha$ for the total angle of attack $\alpha_0 \pm \Delta\alpha$ is negative in general (Den Hartog 1932). However, for small p, condition (2) is usually not met (partly due to bearing friction) until a critical initial value of p is reached.

The relation between initial impulse and final rate of autorotation may be illustrated more clearly by a method developed by Riabouchinsky (1935): A motor drives the propeller with constant angular velocity Ω, and the torque T acting on the propeller is measured as a function of p. The resulting curve is shown in Figure 6. When p is small or large, an outside positive torque is necessary to drive the propeller. Between these values, a p-range exists in which the outside torque is negative and thus requires a braking effect on the rotation of the propeller. Riabouchinsky called this range "autorotative." If the outside torque is removed, the propeller increases its angular velocity until $T = 0$, which is the state of autorotation (point A in Figure 6). The second state $T = 0$, which is the initial value of p needed to induce autorotation, is unstable. The conditions for stable autorotation are thus

$$T = 0, \qquad \frac{dT}{dp} > 0. \tag{3}$$

Although the functioning of the Lanchester propeller has been demonstrated many times, there appears to be only one experimental investigation that provided quantitative data, that by Parkinson (1964). He found that in the Reynolds-number range $2800 < \mathrm{Re} < 1.6 \times 10^5$, with R the tip radius, ν the kinematic viscosity, and $\mathrm{Re} = RU/\nu$, the value p for stable autorotation is almost independent of Re and is between approximately 1.96 and 2.16 for a D-shaped blade. The initial value of p for the onset of autorotation is about 0.5. However, friction of the shaft must be taken into account.

Parkinson computed p by means of the steady-state strip theory and used experimental data for L and D. He obtained $p = 1.79$ for stable

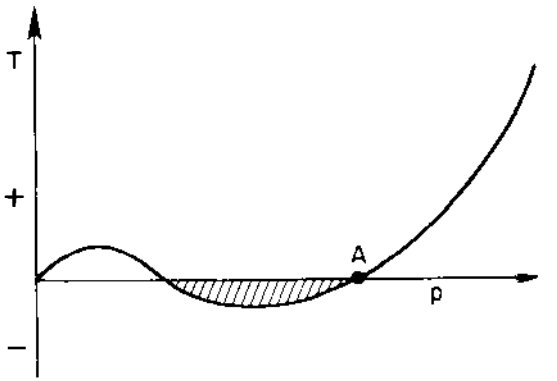

Figure 6 "Riabouchinsky curve" for the explanation of autorotation. A is the point of stable autorotation.

autorotation and $p = 0.45$ for the initial value. Hence the stable rate of rotation is underestimated by the theory by 9% to 17%. Clearly, the neglect of three-dimensional effects is the main reason for this discrepancy. Parkinson (1964) pointed out that centrifugal effects would shift the midsection of the propeller farther out with a torque favorable to autorotation and thus increase p.

3.2 *Autorotating Wing*

The explanation for a wing autorotating about a fixed axis parallel to the flow (Figure 2*b*) is basically the same as that for the Lanchester propeller. The angle of attack of a wing element on the downward-moving half of the wing is $\alpha_0 + \Delta\alpha$, whereas the angle of attack of the corresponding wing element on the upward-moving half is $\alpha_0 - \Delta\alpha$. Stall at $\alpha_0 + \Delta\alpha$, i.e. a negative $dL/d\alpha$, may cause a torque in the direction of rotation. But the problem here is more involved; since α_0 is not restricted to one value (90° for the Lanchester propeller), it is now a parameter, ranging from ca. 0° to values far into the stall region. Discussion of the influence of various values of α_0 on autorotation gives more insight into the nonlinear behavior of this phenomenon.

Extending Riabouchinsky's curve in Figure 6 to a family of curves with α_0 as a parameter, one obtains Figure 7. Glauert's (1919) theoretical data for a RAF 6 wing have been depicted as a typical example. Notice that autorotation can occur for $p \ll 1$ and that p is much smaller for the autorotating wing than for the Lanchester propeller. In Figure 8, the roll

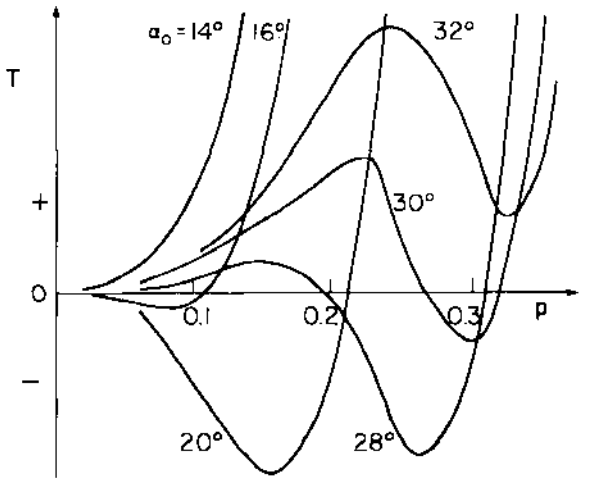

Figure 7 The torque of a rotating wing as a function of p and α_0 (adapted from Glauert 1919).

parameter p for autorotation is plotted versus the angle of attack α_0. The lowest value of α_0 for nonzero p is at 15°, close to the stall angle. Below this value the wing is stable for $p = 0$; beyond, it is unstable for $p = 0$. The latter result implies that a nonrotating wing can start autorotating at the slightest rotational disturbance. From approximately 26.5° to 31.5°, two equilibrium states for $p \neq 0$ occur as in the case of the Lanchester propeller. The smaller value of p is unstable, the larger stable.

The curves in Figures 7 and 8 differ, of course, for other wing profiles and flow situations. Negative $dL/d\alpha$, for instance, can occur for delta wings when the vortex lift drops because of vortex breakdown over the wing area (Küchemann 1978).

The computation of the characteristics of autorotating wings today is still based on the steady-state strip approach with the aid of empirical data for a wing element. According to Glauert (1919), the accuracy is about 15%, that is, on the order of Parkinson's (1964) findings for the Lanchester propeller.

Figures 7 and 8 and Glauert's condition (2) indicate that the problem of autorotation is nonlinear. This is not surprising since stall is the cause of autorotation. Figure 8, by the way, is a familiar curve in catastrophe theory (Zeeman 1977), and condition (2) can be derived from a power-series solution of the nonlinear-oscillator equation (Parkinson 1974).

The yawing motion of the fuselage of an airplane can lead to autorotation. This phenomenon is based on the same principle as that of the roll of a wing becoming self-sustained. This observation is important for the understanding of freely spinning airplanes, which is discussed in Section 5.

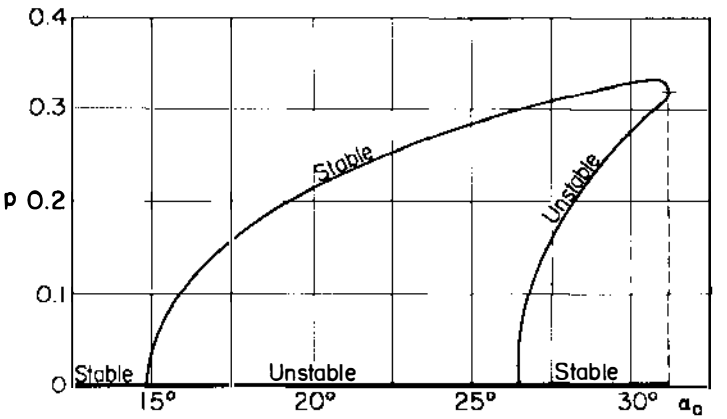

Figure 8 The rate of autorotation p, obtained from Figure 7, as a function of α_0 (adapted from Glauert 1919).

4. AUTOROTATION PERPENDICULAR TO THE FLOW

The fundamental difference between autorotation parallel to and autorotation normal to the flow is that the rate of stable autorotation is constant in the first case and periodic in the second. This difference affects the definition of autorotation: The torque T and angular velocity Ω (or p) in Equation (3) must be replaced by the corresponding quantities averaged over one cycle, where a body with n-fold axial symmetry has a cycle of period $2\pi/n$. Thus, the average torque $\overline{T}$ for use in the definition of stable autorotation is

$$\overline{T} = \frac{n}{2\pi} \int_0^{2\pi/n} T \, d\alpha, \tag{4}$$

where

$$T = I \frac{d\Omega}{dt} \tag{5}$$

with I the moment of inertia and t the time.

A consequence of the difference in characteristics between autorotation parallel to and normal to the flow is that in the latter case, when the axis is kept fixed, steady-flow models with empirical ("static") data cannot be used unless they are introduced in a "quasi-steady" sense. "Quasi-steady" means that the forces on the body vary so slowly with rotation that they can be computed at a particular instant as if the body were not rotating. Even then it is easy to see that a quasi-steady approach always results in $\overline{T} = 0$, except when static hysteresis or a sudden drop in the force coefficient at increased speed occurs. Static hysteresis means a hysteresis effect occurring from one steady state to another in contrast to "dynamic hysteresis" of an accelerated body (Ericsson & Reding 1969). For an autorotating body with freely moving axis, the quasi-steady model may be useful under certain restrictions (see Section 4.2). In general, a strip theory cannot be applied to bodies autorotating normal to the flow since the whole wake region periodic in time must be considered.

The following discussion of two examples (Sections 4.1 and 4.2) illustrates the role and applicability of the concepts introduced here in more detail.

4.1 Rotating Dumbbell

Not much is known about the rotating dumbbell depicted in Figure 3*a*. The explanation for autorotation is based on the sudden drop of the drag coefficient of a sphere at the transition from laminar to turbulent flow

near $\mathrm{Re} = 2RU/\nu = 4 \times 10^5$, with R the radius of the sphere (A. M. O. Smith 1953). The effective velocity of the sphere advancing in the main stream is larger than that of the retreating sphere, yet the latter sphere experiences a larger drag since it is still in the laminar flow range (Eiffel-Prandtl paradox). This quasi-steady approach for explaining the autorotation of dumbbells may be classified as one within the framework of strip theory: the two spheres are the only elements.

Two parallel, long circular cylinders attached to each other by a thin rod can be used instead of two spheres, since the drag curve for the cylinder exhibits the same sudden drop at about $\mathrm{Re} = 4 \times 10^5$.

Except for an experiment with rotating dumbbells cited by A. M. O. Smith (1953), no empirical data are available, nor are technical applications known. The rotating dumbbell will probably remain a curious aerodynamic toy that easily demonstrates the Eiffel-Prandtl paradox.

4.2 *Flat Plate Rotating Perpendicular to the Flow*

A simple experiment demonstrates the capability of a flat plate to autorotate: Cut out a rectangular strip of paper, say 1 cm × 10 cm, and drop it by releasing the strip from a horizontal position, tilted slightly chordwise. The paper will fall along an oblique, straight (slightly undulating) trajectory with rapid rotation normal to the flight path (Figure 9). A deviation from the initial horizontal position (or small mass asymmetry), however, will result in autorotation along a helical flight path. Still, it is not difficult to keep the paper horizontal enough to provide directional stability.

A flat plate that is free to rotate about a fixed axis in the airstream of a wind tunnel can also autorotate under certain conditions.

Extensive experiments under both free-fall and wind-tunnel conditions were made by Dupleich (1941), Cheng (1966), Bustamante & Stone

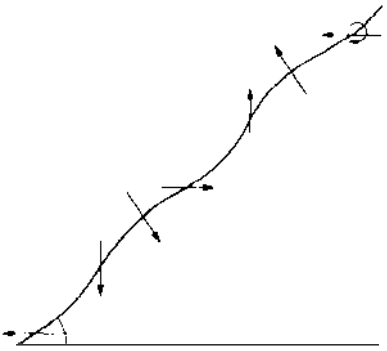

Figure 9 The path of a falling, autorotating plate.

(1969), E. H. Smith (1971), and Glaser & Northup (1971). Most of the experimental data obtained by these researchers have been evaluated and summarized by Iversen (1979).

Free-fall and wind-tunnel data reveal that a certain moment of inertia I is required for a plate to autorotate. The roll parameter p increases with larger values of I but becomes almost independent of I for $I/\rho bc^4 > 1$, where ρ, b, and c are the density of the fluid, span, and chord length, respectively (Iversen 1979). In this region of independence, the difference between free-flight and wind-tunnel autorotation becomes indistinguishable.

With inertia effects no longer considered, the dependence of p on aspect ratio, plate thickness, and Reynolds number, as well as lift and drag behavior, remains to be discussed.

Iversen (1979) offers the following formula based on experimental data for the influence of the aspect ratio $A = b/c$ on p:

$$p = \left\{ \frac{A}{2+\sqrt{4+A^2}} \left[2 - \left(\frac{A}{A+0.595} \right)^{0.76} \right] \right\}^{2/3}, \tag{6}$$

where the relative thickness of the plate (defined by thickness/c) is smaller than 0.01. For $A > 5$, the influence of A on p can be ignored, and this restriction can be relaxed with the aid of endplates.

The relative thickness has a negligible effect on p for values less than 0.01. For thick plates and fat noncircular cylinders, the roll parameter p decreases. Autorotation of circular cylinders has never been observed.

The roll parameter is nearly independent of the Reynolds number for $\mathrm{Re} = cU/\nu > 1500$ and is about 0.8–1.0 for thin plates and large aspect ratios. Numerical and measured data as low as $\mathrm{Re} = 100$ indicate a drop in p for such small Re (E. H. Smith 1971, Lugt 1980). When $\mathrm{Re} \to 0$, autorotation ceases.

Almost all experiments have been made for subsonic flows. Bustamante & Stone (1969) found evidence for autorotation in supersonic flow, but little is known about this flow region.

The lift-to-drag ratio, which equals the cotangent of the glide angle, increases with increasing p. Iversen (1979) correlated the empirical data of Dupleich for L/D with p and other flow parameters in a graph that displays measured values for L/D in the interval (0.4, 1.6). A rule of thumb was presented earlier by Iversen (1969) in the form $L/D = c_L/c_D = 1.4p$, which is based on $p^2 = A/8$, $c_D = 2$, $c_L = A^{0.5}$ for $A < 8$ where $c_D = D/(\rho/2)U^2bc$, and c_L is defined correspondingly.

Instantaneous flow quantities, such as force and moment coefficients at a certain instant, and the surface pressure have been measured by

Cheng (1966) and E. H. Smith (1971). Cheng published for the first time the distribution of the surface pressure along the chord of a rotating plate and data for the aerodynamic torque. The main novel features in E. H. Smith's experiments are recorded data on the instantaneous lift and drag coefficients.

The experimental difficulties in obtaining reliable data should be noted. In addition to problems of reducing bearing friction, which every experimentalist in this field has encountered, measurement of the instantaneous aerodynamic loading on the rotating plate caused difficulties. Cheng (1966) used 13 pressure taps at midspan, a sliding pressure seal, and a pressure transducer. Essentially the same arrangement but with a different sliding-seal mechanism was used by Miller (1973, 1979). E. H. Smith (1971) mounted strain gauges on one of the bearing supports to measure lift and drag. Data on the instantaneous distribution of the surface pressure and torque for a freely falling plate do not exist. Their acquisition would be a challenge for any experimentalist!

Theoretical explanations of the autorotating plate started with Maxwell (1890) in 1853 for the case of the freely falling plate. He recognized that the center of mass and the center of aerodynamic forces do not coincide, giving rise to a torque. He then assumed that this torque can be divided into a quasi-steady part and a contribution due to rotation. The latter, Maxwell believed, would always have a damping effect. From $\alpha = 0°$ to 90° the torque on the plate supports rotation ("supporting period"), whereas from $\alpha = 90°$ to 180° the torque acts on the plate in opposition to rotation ("retarding period"). Maxwell recognized that the torque in the supporting period is larger than in the retarding period because the translational velocity of the plate for $\alpha = 0°$ is larger (the drag is smaller) than that for $\alpha = 90°$. The higher translational speed around $\alpha = 0°$ causes a larger torque in the supporting period. This driving net torque would be balanced, according to Maxwell, by the damping effect of the rotation.

Maxwell's argument is only partially correct, and this only when the amplitude of the undulatory path of the plate's axis (Figure 9) is sufficiently large. However, with increasing moment of inertia the amplitude decreases, and the difference between free-fall and fixed-axis autorotation vanishes. The quasi-steady model ceases to be valid, and the rotational effect must be considered to support autorotation. This concept is explained in the paragraphs that follow (Lugt 1980).

In potential-flow theory, the torque coefficient $c_M = T/(\rho/2)U^2(c/2)^2$ acting on a plate with a fixed axis depends only on α (and not explicitly on Ω), whether it rotates or not:

$$c_M = -\pi \sin 2\alpha, \tag{7}$$

where α is either a constant or time-dependent, i.e. $\alpha = \Omega t$. The average torque is zero, and the plate always autorotates. This solution is not useful for explaining autorotation, but it reveals the importance of the existence of the supporting and retarding periods caused by the asymmetric locations of the stagnation points.

Viscous effects must be taken into account. Numerical computations with the Navier-Stokes equations reveal the following relationship between instantaneous torque and flow patterns: In Figure 10 the torque coefficient c_M of a thin elliptic cylinder is displayed as a function of α for various values of p at Re = 200 (p constant in time). Drastic changes for different p occur in the retarding period near $\alpha = 135°$. If one averages c_M and plots it versus p, one obtains Riabouchinsky's curve of Figure 6 (Lugt 1980). Clearly, the deviation of curves in Figure 10 from the sinusoidal behavior in the retarding period is related to the "autorotative" region in Figure 6.

A comparison of computed and photographed flow patterns reveals that this "autorotative" region coincides approximately with the synchronization of vortex-shedding frequency and rate of rotation, a manifestation of the nonlinear "lock-in" effect. The situation is sketched in Figure 11*b* for the decisive α-range of about 135°. For values of p outside the autorotative region, the frequency of vortex shedding is either smaller

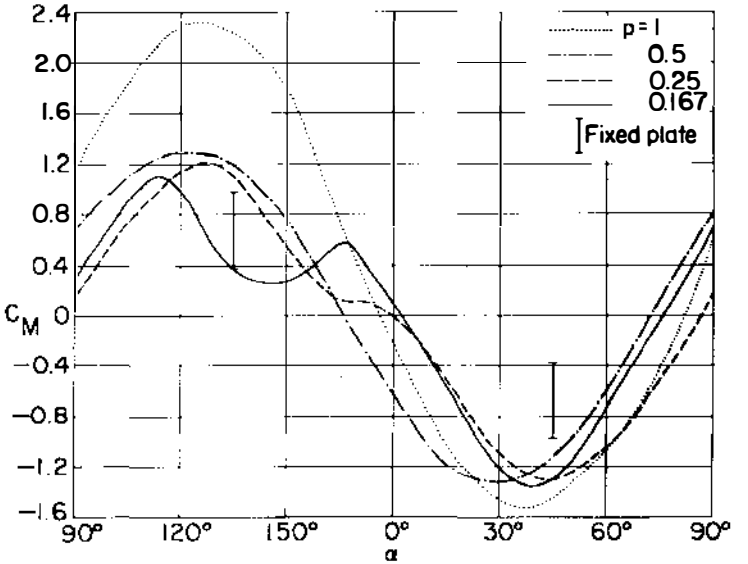

Figure 10 Comparison of c_M versus α for various p over one cycle (half-revolution of the plate) at Re = 200 (from Lugt 1980).

(Figure 11*a*, superharmonic modes) or larger (Figure 11*c*, subharmonic modes) than the rate of rotation. The superharmonic modes differ by integral values from each other, a fact that has a simple physical explanation: a rapidly rotating plate traps vortices before it releases them after several revolutions. The trapping of vortices over a small range of p constitutes a lock-in at higher harmonics, a phenomenon observed in vortex-induced vibration (Ericsson 1980; see also Section 6). In the subharmonic range, the vortex-shedding frequency approaches that of a nonrotating plate when $p \to 0$ and becomes independent of the slow rate of rotation.

For autorotation, the flow patterns are essentially independent of the Reynolds number and are even similar for the laminar and turbulent states. The inertial forces due to the periodic change of the flow field do not give sufficient time for the diffusion of vorticity or the small-scale turbulent eddies to have a significant influence on the overall process.

The reason for autorotation becomes evident when the surface pressure in the retarding period is compared with that in the supporting period for various p. Near $\alpha = 135°$, the vortex at the retreating edge (which is very pronounced in wind-tunnel movies made by the Aerodynamics Department at the University of Notre Dame) has just separated from the body for $p \approx 0.25$ (Figure 11*b*), and the flow around the edge looks similar to the flow past a plate parallel to the stream. The surface pressure and vorticity are almost symmetric on the two rear halves of the plate (Figure 12), which means that the surface pressure is quite constant on both sides of the plate. In contrast, for higher as well as lower p, the front surface pressure near the retreating edge is very low (in qualitative agreement with potential flow) and thus counteracts autorotation. Computations confirm that the average torque in the retarding period has a minimum in the autorotative range (area under the c-curve for $p = 0.25$ in the α-range $[90°, 0°]$ in Figure 10). This strange behavior does not occur in the supporting period, in which the average torque is almost constant. Details of the delicate balance between the torque contributions of the retarding and supporting periods are given in Lugt (1978, 1980).

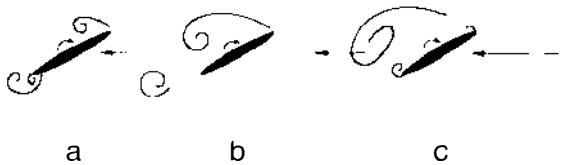

Figure 11 Sketch of vortex shedding about a power-driven rotating plate. (*a*) p is greater than that for autorotation; (*b*) lock-in range of p (autorotative); (*c*) p is slower than that for autorotation.

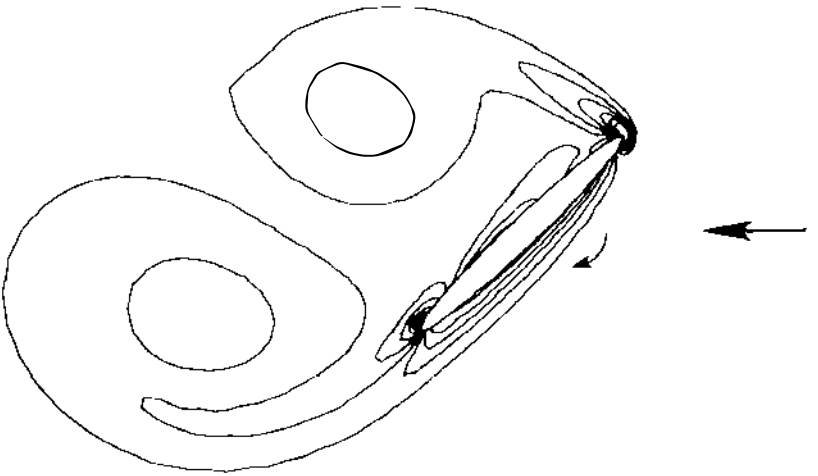

Figure 12 Equivorticity lines for Re ≈ 200, $p = 0.25$, $\alpha = 135°$.

For two-dimensional freely falling plates and for autorotating plates of finite span (three-dimensional flow), computations are not known to exist. A decrease in autorotation due to three-dimensional effects, observed experimentally and expressed in Equation (6), is caused by the weakening of the shed vortices. Considering the vortices idealized by vortex tubes in a potential flow, one realizes that a body with finite span is surrounded by a flow in which the vortex tubes are either closed or must end on the body. They are bent at the ends of the plate, thus giving rise to a secondary flow. This flow interferes with the primary (two-dimensional) flow by weakening it in two ways: by decreasing the strength of the primary flow, and by speeding up the process of instability, since curved vortex tubes are highly unstable in general.

4.3 Other Autorotating Devices

The flat plate and the thin elliptic cylinder are by no means the only cylindrical bodies capable of autorotation. Other shapes like cruciform plate arrangements, triangles, and squares can autorotate (Figure 3*c*). Riabouchinsky (1935) experimented with triple and cruciform plates, and he found that the rate of rotation decreases with increasing number of plates. The number of plates at which autorotation ceases is not yet known.

These cylindrical bodies belong to the general class of Magnus rotors that are defined as cylindrical bodies of fairly arbitrary cross section, designed for fast spinning. The name is derived from the Magnus effect of producing lift through rotation. Magnus rotors also include bodies

whose self-sustained spinning has been labeled in Section 2 as "pseudo-autorotation" (Figure 1). The numerous publications include papers by Flatau (1964), Yelmgren (1966), Stilley (1967), Gebman (1967), Brunk (1967), Iversen (1969), and Miller (1979).

Obviously, p is larger for asymmetric rotor devices of the types depicted in Figure 1 than for symmetric devices. The Savonius rotor appears to have the highest value of p among the Magnus rotors investigated (Yelmgren 1966, Iversen 1969), i.e. $p = 1.37$ for $A = 1.45$ and Reynolds numbers of the order 10^5. (A theoretical upper limit is $p = 2$, based on potential flow around a rotating circular cylinder and on the criterion of the occurrence of closed streamlines.) The Darrieus rotor is mentioned in this context as a device that is not a Magnus rotor. Its blades whirl around the center, similar to the cylindrical dumbbell but with very high values of p up to 7. (Strickland et al. 1979). It is conjectured that the Darrieus rotor also works for blades with fore-aft symmetry. The motion would then constitute autorotation proper.

Bodies need not be cylindrical to be able to autorotate. Riabouchinsky (1935) mentioned airships that can autorotate perpendicular to the flow. A. M. O. Smith (1953) was originally motivated in his research by the autorotation of nose sections of aircraft that can be released in an emergency. Reentry bodies and spacecraft can autorotate when diving into the atmosphere, a situation that must be avoided by all means. (Astronauts Glenn and Carpenter could prevent their Mercury capsule from autorotation only by opening the parachute.) Disk-shaped bodies can also autorotate, as demonstrated by a coin falling in water (Willmarth et al. 1964) or a discus thrown without a spin in the azimuthal direction (Soong 1976). Hailstones are also able to autorotate (Kry & List 1974a, b, List et al. 1973). Calculations for a rotating discus and for hailstones were based on the quasi-steady approach with the aid of empirical static data.

The problems and major issues today involving bodies autorotating perpendicular to the flow are summarized as follows:

1. Accurate performance prediction requires better knowledge and correlation of wind-tunnel and free-fall data for p, L/D, and directional stability as functions of the various parameters involved.
2. Local and instantaneous aerodynamic force characteristics are needed.
3. For freely falling autorotating bodies, the limits of applicability of the quasi-steady approach must be studied.
4. For powered Magnus rotors, sub- and superharmonic modes need to be determined.

5. AUTOROTATION AT ARBITRARY ANGLE TO THE FLOW

The difficulties encountered in Sections 3 and 4 in explaining and computing autorotation parallel to and normal to the flow are magnified considerably for bodies that autorotate at an arbitrary angle to the flow. Here, the differences in flow characteristics between rotation about a fixed and a freely moving axis (free flight) become decisive compared with the previously discussed cases. In free flight the body performs motions with six degrees of freedom, and gyroscopic effects are therefore present.

It has been stated in Sections 3 and 4 that the torque on a body rotating about a fixed axis depends on p as expressed by the Riabouchinsky curve (Figure 6). A qualitative polynomial representation of this relation is

$$c_M = c_1 p + c_3 p^3 + c_5 p^5, \tag{8}$$

where the coefficients c_i are constants. In certain regions a cubic relation suffices (Figure 7).

The physical meaning and the magnitude of the coefficients c_i can be obtained either by a strip theory with static-force data or by solutions of the Navier-Stokes equations for the special cases discussed in Sections 3 and 4.

Such an interpretation of the "global" aerodynamic coefficients c_i with detailed knowledge of the local flow field is not yet possible for the three-dimensional motion of bodies in free flight or rotating about fixed axes. These problems are simply too complex. Instead, only measured data of global force and moment components (like the moments of roll, yaw, and pitch) can be correlated to the aerodynamic coefficients. Before discussing this further, attention is drawn to the coupling among rolling, yawing, and pitching motions through unequal moments of inertia in free flight. For instance, the roll moment c_M is balanced in steady roll according to the Euler equations by the "inertia coupling"

$$c_M = (C - B)qr, \tag{9}$$

where q and r are the rates of pitch and yaw, and B and C are the dimensionless moments of inertia about the transverse y-coordinate and the vertical z-coordinate, respectively.

A common practice in aerodynamics is to consider only linear damping for c_M. Sometimes aerodynamic coupling analogous to the inertia coupling is included. Apparently, fifth-order polynomials of the form of Equation (8) are not necessary to demonstrate autorotation. However, it

is clear that linear damping and quadratic coupling only must be applied with caution.

Another question arises on whether experimental aerodynamic static data suffice for correlation with the aerodynamic coefficients, or whether rotary data must be used, as shown for certain instances by Anglin (1978) and Langham (1978).

The following discussion is limited to two cases of great engineering interest: (*a*) the spinning and rolling of aircraft, and (*b*) the autorotation of finned missiles. It must be stressed, however, that these subject areas can be discussed only briefly within the scope of this review because of the vast amount of existing literature.

5.1 Autorotation of Spinning and Rolling Aircraft

When an airplane is stalled asymmetrically, either unintentionally or on purpose, it may descend nose-down in a rolling and yawing motion on a spiral path at an angle of attack between stall and 90° (Figure 13). This phenomenon is called "spin" (Jones 1963).

Airplanes have been troubled by spin from the time they came of age (about 1909). At the end of World War I the phenomenon of spin (and recovery from it) was understood in principle (Lindemann et al. 1918, Relf & Lavender 1918, Glauert 1919), although total avoidance of spin

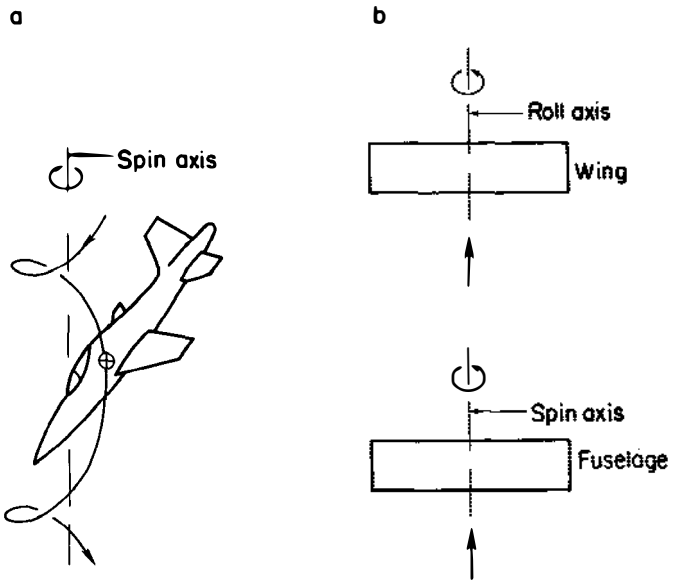

Figure 13 (*a*) Spinning airplane; (*b*) pure rolling and pure yawing motions.

was not achieved in the succeeding decades. The problem persists today for light commercial airplanes because of their relatively greater engine power (Bowman 1971, Anderson 1979), and it is even aggravated in modern fighter aircraft (Anglin 1978) because of their greater weight, swept wings, and jet engines (see below). After all, maneuverability and stability of aircraft are incompatible in a way.

Aerodynamicists distinguish three phases of spin: (*a*) spin entry, (*b*) equilibrium spin, in either a steady or oscillatory mode, and (*c*) spin recovery. Only the second phase with all control surfaces in neutral positions is autorotation proper. "Flat spin" and "steep spin" are distinguished by the angle θ of the longitudinal axis of the airplane with the vertical. In a flat spin the angle θ is larger than 80°; in a steep spin it is $45° < \theta < 75°$. According to the relation $r_0 S^2 = g \cot \theta$, where S, r_0, and g are the rate of spin around the spin axis (not the rate of roll), the radius of the helical path, and the gravitational constant, respectively, a small value of r_0 in flat spin results in a large value of S (which for θ close to 90° is essentially a yawing motion with S on the order of half a revolution per second). A larger value of r_0 in steep spin decreases S.

Spin may be considered roughly as a combination of two autorotation effects (Figure 13): roll of the wing, as described in Section 3.2, and yawing of the fuselage, where the fuselage may be regarded as a wing or a Lanchester propeller, especially for flat spin (Clarkson 1958, Clarkson et al. 1978).

The influence of the fuselage on spin becomes crucial in modern fighter planes with their long fuselage nose and heavy fuselage mass loadings. According to Neihouse et al. (1960), the moments of inertia about the *y*- and *z*-axes are an order of magnitude larger than those of World War II airplanes. In addition, swept wings have a negative influence on longitudinal and rolling stability. Steady spin at high angles θ can change at lower angles to oscillatory spin (Skow & Titiriga 1978) with typical "limit cycle" behavior (Mehra & Carroll 1979). Near stall the phenomenon of "wing rock" can occur, caused by aerodynamic roll moment hysteresis (Schmidt 1979). Also, spin entry is facilitated by asymmetric vortex shedding from the nose of the aircraft (Spangler & Mendenhall 1977) or by vortex breakdown over delta wings.

The design of modern aircraft has led to the discovery of another kind of autorotation that can occur during fast rolling maneuvers. Again, inertia forces of high-speed aircraft cannot be neglected, and they tend to swing the fuselage out of the flight path (Phillips 1948). This sideslipping causes coupling of longitudinal and lateral gyroscopic and aerodynamic characteristics, similar to spin. However, in contrast to spin, rolling motion involves much higher values of p and the flight path is essentially

horizontal. Pinsker (1957) has shown that this rolling with sideslip can become self-sustained without asymmetrical moments enforced by the aileron; he called this situation "autorotation in roll." Nonlinear inertia cross-coupling and linear aerodynamic damping are sufficient to demonstrate the existence of autorotation in roll for a certain parameter range. However, a recent paper by Sachs & Fohrer (1980) shows that additional aerodynamic coupling, through introduction of rolling moments due to angle of attack and sideslip and of quadratic terms of pitching moments due to angle of sideslip, has a strong influence on autorotation. This is an example of the importance of the correct polynomial representation of the aerodynamic coefficients for the realistic description of autorotation.

Cohen & Nimri (1976) investigated rolling delta wings by including leading-edge vortices in their model.

5.2 *Roll Speed-Up of Finned Missiles*

Three regimes of steady rotation are distinguished for the rolling motion of finned missiles in free flight, depending on the angle of attack α, which is here defined as the angle between flow and horizontal missile axis in Figure 4 (Nicolaides 1957). For convenience, only the cruciform-fin configuration is considered.

For small angles of attack greater than $\alpha = 0°$, steady roll can be maintained only by canted fins. This region is called "roll slow-down," because p decreases with larger α until a situation is reached at which the fins are locked with the coning motion of the missile. This situation, which occurs for canted as well as uncanted fins, is therefore called "roll lock-in" or "lunar motion" and extends up to about $\alpha = 36°$. Beyond this value up to 90°, p drastically increases and reaches a value of 0.25 at 90° for uncanted fins with Re of the order of 10^5. This region of steady roll is called "roll speed-up" and is the only region of autorotation proper.

In contrast to "autorotation in roll" and equilibrium spin of aircraft for which yawing and pitching are essential to explain autorotation, finned missiles can autorotate without yawing and pitching. This fact and the extreme complexity of the flow field around a missile in free flight resulted in studies that are mostly devoted to a missile autorotating about a fixed axis in a wind tunnel.

Experiments have shown (Greene 1960) that roll speed-up about a fixed axis occurs whether the cruciform fins are attached to the body or disconnected, and even without a body. It was conjectured by Nicolaides (1957) that roll speed-up was similar to wing autorotation, although not exactly the same, and Greene (1960) suspected a "special kind of autorotation." Looking at the simplest case of $\alpha = 90°$, Lugt (1961)

interpreted roll speed-up as the same phenomenon as plate autorotation normal to the flow (Figure 3*b* and *c*, Section 4.2).

As in the case of spin and roll of aircraft, analysis of roll speed-up can be done at present only by correlating experimental data with aerodynamic coefficients. Whereas for spin and roll of aircraft, inertia coupling is essential for steady autorotation and provides solutions with linear damping only (whether this is realistic or not), roll speed-up about a fixed axis requires the fifth-order polynomial of Equation (8) in general, or at least a third-order one for certain parameter regions. This follows from the interpretation of reducing roll speed-up to plate autorotation. It is interesting that Daniels (1970) and Cohen et al. (1974) needed third-order polynomials to correlate experimental data with the aerodynamic coefficients. Other work on nonlinear damping was reported by Uselton & Jenke (1977).

For finned missiles below $\alpha = 40°$, vortices shed from the body may interfere with the fins. In fact, Nicolaides (1957) used this argument to explain roll lock-in. A more recent paper on autorotation with body-vortex interference was published by Fiechter (1972). Papers on rotating missiles in free flight have included those by Murphy (1971) and Clare (1971).

6. ANALOGY TO VORTEX-INDUCED VIBRATION

Den Hartog (1932) was probably first to call attention to the analogy between the Lanchester propeller and a special kind of vibration labeled as "galloping" and observed on cables. This vibration is characterized by the property that the reduced frequency (which is the ratio of oscillation frequency times characteristic length to parallel-flow velocity) is much smaller than unity, and hence a quasi-steady strip theory for computing the side force can be applied. In fact, this strip theory for blade elements is the same for the Lanchester propeller and galloping, including Glauert's condition in Equation (2). Den Hartog even suggested the Lanchester propeller as a simple test apparatus for studying various cable cross sections for their galloping behavior. The only difference between the Lanchester propeller and galloping is that the motion of the former is steady, whereas the latter is slowly oscillatory.

Analogies and similarities also exist between vortex-induced vibration for unrestricted values of the reduced frequency and rotation of plates normal to the flow:

1. Lock-in or synchronization near the natural (linear) resonance frequency.
2. Energy transfer from the fluid flow to the body.

3. Existence of sub- and superharmonic modes for forced vibration and rotation.

These properties of vibrating and rotating bodies in a parallel flow are typical of nonlinear coupled oscillators, which can be described, for instance, by the van der Pol equation for the side force of a vibrating body coupled with an equation for the body motion. A huge amount of literature on various types of these ordinary differential equations exists (Sarpkaya 1979), almost all of it dealing with translational vibration normal to the flow. A common description of rotational oscillation and rotation could be achieved by extending the restoring moment $c\alpha$ to $c \sin \alpha$ and thus obtaining pendulum-type equations. The author knows of no such studies.

The nonlinear-oscillator model is, of course, a mechanical analog for a qualitative description of a fluid-dynamical phenomenon. But it is not a model in the sense of an approximation to the aerodynamic field equations (which are partial differential equations). In that respect, the nonlinear-oscillator model will always be deficient, and the proper approach will be the solution of the field equations (Sarpkaya 1979). This statement is also true for the problems connected with autorotation.

ACKNOWLEDGMENTS

The author would like to thank Mr. H. Cheng from DTNSRDC for fruitful discussions and Mrs. A. Phillips for her contribution to the readability of this article. The preparation of the manuscript was supported by the Independent Research Program at DTNSRDC.

Literature Cited

Anderson, S. B. 1979. Historical overview of stall spin characteristics of general aviation aircraft. *J. Aircr.* 16:455–61

Anglin, E. L. 1978. Acrodynamic characteristics of fighter configurations during spin entries and developed spins. *J. Aircr.* 15:769–76

Bowman, J. S. 1971. Summary of spin technology as related to light general-aviation airplanes. *NASA-TN-D-6575*. 34 pp.

Brunk, J. E. 1967. Aerodynamics and flight mechanics of high performance autorotating glide-type bomblets. In *Proc. Conf. Dyn. Aerodyn. Bomblets*, Vol. 1. *Tech. Rep. AFATL-TR-67-195*, Eglin AFB, Fla.

Burgess, F. F., ed, 1967. *Proc. Conf. Dyn. Aerodyn. Bomblets*, Vol. 1. *Tech. Rep. AFATL-TR-67-195*, Eglin AFB, Fla.

Bustamante, A. G., Stone, G. W. 1969. The autorotation characteristics of various shapes for subsonic and hypersonic flows. *AIAA Pap. No. 69-132*

Cheng, H. 1966. *An experimental investigation of the autorotation of a flat plate.* MASc thesis. Univ. Br. Columbia. 103 pp.

Clare, T. A. 1971. Resonance instability for finned configurations having nonlinear aerodynamic properties. *J. Spacecr.* 8:278–83

Clarkson, M. H. 1958. Autorotation of fuselages. *Aeronaut. Eng. Rev.*, Feb., pp. 33–36

Clarkson, M. H., Malcolm, G. N., Chapman, G. T. 1978. A subsonic, high-angle-of-attack flow investigation at several Reynolds numbers. *AIAA J.* 16:53–60

Cohen, C. J., Clare, T. A., Stevens, F. L. 1974. Analysis of the nonlinear rolling motion of finned missiles. *AIAA J.* 12:303–9

Cohen, M. J., Nimri, D. 1976. Aerodynamics of slender rolling wings at incidence in separated flow. *AIAA J.* 14:886–93

Daniels, P. 1970. A study of the nonlinear rolling motion of a four-finned missile. *J. Spacecr. Rockets* 7:510–12

Den Hartog, J. P. 1932. Transmission line vibration due to sleet. *Trans. AIEE* 51:1074–86

Duplcich, P. 1941. Rotation in free fall of rectangular wings of elongated shape. *NACA Tech. Memo. 1201*

Ericsson, L. E. 1980. Kármán vortex shedding and the effect of body motion. *AIAA J.* 18:935–44

Ericsson, L. E., Reding, J. P. 1969. Unsteady airfoil stall. *NASA CR-66787*, Lockheed, Sunnyvale, Calif.

Fiechter, M. 1972. Kegelpendelung, Autorotation und Wirbelsysteme schlanker Flugkörper. *Z. Flugwiss.* 20:281–91

Flatau, A. 1964. An investigation of the rotational and aerodynamic characteristics of high aspect ratio rotors. *CRDL TM 1-4*, Edgewood Arsenals, Md.

Gebman, J. R. 1967. A description of the rotational characteristics of high aspect ratio modified rectangular rotors. In *Proc. Conf. Dyn. Aerodyn. Bomblets*, Vol. 1. *Tech. Rep. AFATL-TR-67-195*, Eglin AFB, Fla.

Glaser, J. C., Northup, L. L. 1971. Aerodynamic study of autorotating flat plates. *Rep. ISU-ERI-Ames 71037.* Eng. Res. Inst., Iowa State Univ., Ames

Glauert, H. 1919. The rotation of an aerofoil about a fixed axis. *Advisory Committee for Aeronautics, Rep. and Memo. No. 595*, March, pp. 443–47

Greene, J. E. 1960. An investigation of the rolling motion of cruciform-fin configurations. *NAVORD Rep. 6262*

Iversen, J. D. 1969. The Magnus rotor as an aerodynamic decelerator. *Proc. Aerodyn. Deceleration Syst. Conf.*, 2:385–95. Air Force Flight Test Cent., Edwards AFB, Calif.

Iversen, J. D. 1979. Autorotating flat-plate wings: the effect of the moment of inertia, geometry and Reynolds number. *J. Fluid Mech.* 92:327–48

Jones, B. M. 1963. The spin. In *Aerodynamic Theory*, ed. W. F. Durand, Vol. 5. New York: Dover. 347 pp.

Kry, P. R., List, R. 1974a. Aerodynamic torques on rotating oblate spheroids. *Phys. Fluids* 17:1087–92

Kry, P. R., List, R. 1974b. Angular motions of freely falling spheroidal hailstone models. *Phys. Fluids* 17:1093–1102

Küchemann, D. 1978. *The Aerodynamic Design of Aircraft.* Elmsford, NY: Pergamon

Langham, T. F. 1978. Correlation of experimental and theoretical steady-state spinning motion for a current fighter airplane using rotation-balance aerodynamic data. *AIAA Pap. 78-1373*, pp. 325–36

Lindemann, F. A., Glauert, H., Harris, R. G. 1918. The experimental and mathematical investigation of spinning. *Advisory Committee for Aeronautics, Rep. and Memo. No. 411*, March, pp. 716–29

List, R., Rentsch, U. W., Byram, A. C., Lozowski, E. P. 1973. On the aerodynamics of spheroidal hailstone models. *J. Atmos. Sci.* 30:653–61

Lugt, H. J. 1961. Self-sustained spinning of a cruciform fin system. *Proc. 5th US Navy Symp. Aeroballistics.* Vol. 1., Pap. No. 35, Nav. Ordnance Lab., White Oak, Md. 10 pp.

Lugt, H. J. 1978. Autorotation of plates. *David Taylor Nav. Ship Res. Dev. Cent. Rep. 78/058.* 104 pp.

Lugt, H. J. 1980. Autorotation of an elliptic cylinder about an axis perpendicular to the flow. *J. Fluid Mech.* 99:817–40

Maxwell, J. C. 1890. On a particular case of the descent of a heavy body in a resisting medium. *Scientific Papers*, p. 115. Cambridge Univ. Press

McCutchen, C. W. 1977. The spinning rotation of ash and tulip tree samaras. *Science* 197:691–92

Mehra, R. K., Carroll, J. V. 1979. Global stability and control analysis of aircraft at high angles-of-attack. *ADA-084938.* Sci. Syst. Inc., Cambridge, Mass.

Miller, M. C. 1973. A dynamic and aerodynamic analysis of an articulated autorotor decelerator system. *AIAA Pap. No. 73-463.* 15 pp.

Miller, M. C. 1979. Wind-tunnel measurements of the surface pressure distribution on a spinning Magnus rotor. *J. Aircr.* 16:815–22

Murphy, C. H. 1971. Response of an asymmetric missile to spin varying through resonance. *AIAA J.* 11:2197–2201

Neihouse, A. I., Klinar, W. J., Scher, S. H. 1960. Status of spin research for recent airplane designs. *NASA TR R-57*

Neumark, S. 1963. Rotating aerofoils and flaps. *J. R. Aeronaut. Soc.* 67:47–63

Nicolaides, J. D. 1957. On the rolling motion of missiles. *Bur. Ordnance Tech. Note No. 33*

Parkinson, G. V. 1964. On the performance of Lanchester's "Aerial Tourbillion." *J. R. Aeronaut. Soc.* 68:561–64

Parkinson, G. V. 1974. Mathematical models of flow-induced vibrations of bluff bodies. In *Flow-Induced Structural Vibrations*, ed. E. Naudascher, pp. 81–127. New York: Springer. 774 pp.

Phillips, W. H. 1948. Effect of steady rolling on longitudinal and directional stability. *NACA TN 1627*

Pinsker, W. J. G. 1957. Critical flight conditions and loads resulting from inertia cross-coupling and aerodynamic stability deficiencies. *NATO AGARD Rep. 107*

Relf, E. F., Lavender, T. 1918. The autorotation of stalled aerofoils and its relation to the spinning speed of aeroplanes. *Advisory Committee for Aeronautics, Rep. and Memo. No. 549*, Oct., pp. 448–52

Riabouchinsky, D. P. 1935. Thirty years of theoretical and experimental research in fluid mechanics. *J. R. Aeronaut. Soc.* 39:282–348, 377–444

Sachs, G., Fohrer, W. 1980. Einfluss der aerodynamischen Kopplung auf die Flugzeugdynamik bei schnellen Rollbewegungen. *Z. Flugwiss. Weltraumforsch.* 4:379–88

Sarpkaya, T. 1979. Vortex-induced oscillations. *J. Appl. Mech.* 46:241–58

Schmidt, L. V. 1979. Wing rock due to aerodynamic hysteresis. *J. Aircr.* 16: 129–33

Skow, A. M., Titiriga, A. 1978. A survey of analytical and experimental techniques to predict aircraft dynamic characteristics at high angles of attack. *NATO AGARD Conf. Proc. No. 235*, Pap. 19. 37 pp.

Smith, A. M. O. 1953. On the motion of a tumbling body. *J. Aeronaut. Sci.* 20:73–84

Smith, E. H. 1971. Autorotating wings: an experimental investigation. *J. Fluid Mech.* 50:513–34

Soong, T. C. 1976. The dynamics of discus throw. *J. Appl Mech.* 98:531–36

Spangler, S. B., Mendenhall, M. R. 1977. Further studies of aerodynamic loads at spin entry. *Nielsen Eng. and Res. Rep. ONR-CR212-225-3*

Stilley, G. D. 1967. Unified stability criteria for autorotating glide bomblets. In *Proc. Conf. Dyn. Aerodyn. Bomblets*, Vol. 1. *Tech. Rep. AFATL-TR-67-195*, Eglin AFB, Fla.

Strickland, J. H., Webster, B. T., Nguyen, T. 1979. A vortex model of the Darrieus turbine: an analytical and experimental study. *J. Fluid Eng.* 101:500–5

Uselton, B. L., Jenke, L. M. 1977. Experimental missile pitch- and roll-damping characteristics at large angles of attack. *J. Spacecr.* 14:241–47

Willmarth, W. W., Hawk, N. E., Harvey, R. L. 1964. Steady and unsteady motions and wakes of freely falling disks. *Phys. Fluids* 7:197–208

Yelmgren, K. 1966. The autorotation of Magnus rotors. *Dept. Aerosp. Eng. Rep.*, Univ. Notre Dame, South Bend, Ind. 115 pp.

Zeeman, E. C. 1977. *Catastrophe Theory: Selected Papers 1972–1977*. Reading, Mass: Addison-Wesley. 675 pp.